

ChemComm

Chemical Communications

Accepted Manuscript

This article can be cited before page numbers have been issued, to do this please use: C. I. Hiley, C. A. Crawford, M. Senn, R. I. Walton and C. Ritter, *Chem. Commun.*, 2026, DOI: 10.1039/D6CC02124G.



This is an Accepted Manuscript, which has been through the Royal Society of Chemistry peer review process and has been accepted for publication.

Accepted Manuscripts are published online shortly after acceptance, before technical editing, formatting and proof reading. Using this free service, authors can make their results available to the community, in citable form, before we publish the edited article. We will replace this Accepted Manuscript with the edited and formatted Advance Article as soon as it is available.

You can find more information about Accepted Manuscripts in the [Information for Authors](#).

Please note that technical editing may introduce minor changes to the text and/or graphics, which may alter content. The journal's standard [Terms & Conditions](#) and the [Ethical guidelines](#) still apply. In no event shall the Royal Society of Chemistry be held responsible for any errors or omissions in this Accepted Manuscript or any consequences arising from the use of any information it contains.

COMMUNICATION

Direct Solvothermal Crystallisation of the Metastable Cubic Perovskite CsMnF₃ and its MagnetismCraig I. Hiley,^a Catriona A. Crawford,^a Clemens Ritter,^b Mark S. Senn,^{a,*} Richard I. Walton^{a,*}Received 00th January 20xx,
Accepted 00th January 20xx

DOI: 10.1039/x0xx00000x

The solvothermal synthesis of polycrystalline cubic CsMnF₃ at 100 °C is reported, a phase previously prepared phase-pure only at 700 °C and 30 kbar. *In situ* powder X-ray diffraction, shows that cubic CsMnF₃ transforms irreversibly to the 6H polymorph at ~500 °C. The magnetic properties of cubic CsMnF₃ are characterised by G-type antiferromagnetic ordering, as determined from powder neutron diffraction.

The solvothermal synthesis of a wide variety of oxide perovskites has been documented in the literature; this includes various ABO₃ compositions that would usually be expected to crystallise using the high temperatures associated with solid-state chemistry, such as ferroelectric titanates, and niobates, multiferroic chromites and ferrates, magnetoresistive manganites, and superconducting bismuthates.¹ The advantage of direct crystallisation from solution, often under hydrothermal conditions when water is used, is access to materials with small crystallite size (micron to nanometre dimensions) that may be annealed into fine-grained electroceramics, or used in sensing or heterogeneous catalysis because of their high surface areas.²⁻⁴ The synthesis of oxides from solution can also allow access to unexpected polymorphs, either metastable crystal forms that subsequently collapse on further heating, such as the ilmenite structure of NaNbO₃,⁵ or structures usually only stable at higher temperatures, such as the cubic polymorph of BaTiO₃.⁶ Fluoride perovskites have been less studied than their oxide analogues, which may be due to the corrosive nature of many fluoride precursors (fluorine gas or HF, for example) that makes routine synthesis challenging.⁷ Solvothermal routes to metal fluorides offer an attractive way for their convenient preparation, with the use of closed reaction vessels and solution precursors that are easy to handle. Examples include Na₂FeF₄⁸ and NaMF₃ (M = Mn, Fe, Co, Ni),⁹ and oxyfluorides, not accessible by other routes, such as

the M(OH)F diaspores.^{10, 11} Herein we study the solvothermal crystallisation of CsMnF₃ and reveal an example of a polymorph-selective synthesis, where a crystal form previously reported at high temperature and pressure¹² is formed directly under mild conditions. An initial sample of CsMnF₃ synthesised by the solvothermal reaction between the binary fluorides CsF and MnF₂ in ethylene glycol at 160 °C was found to contain mostly the cubic polymorph of CsMnF₃ and some unreacted MnF₂, ~20 wt% of the sample as determined by phase quantification from Rietveld fitting against laboratory XRD (Figure S1a). Increasing the synthesis temperature to 180 °C increased the amount of MnF₂ remaining in the sample, whilst lowering the synthesis temperature revealed a near-linear relationship between temperature and MnF₂ content (Figure S1b), with no significant effect on the crystallinity of the cubic CsMnF₃ phase. Rietveld analysis of the laboratory XRD from a sample prepared at 100 °C suggested that <2.5 wt% MnF₂ is present in this sample. This sample was used in further characterisation experiments (except neutron powder diffraction, see Experimental and below).

Synchrotron powder XRD was collected using beamline I11,¹³ (Diamond Light Source, U.K.) from the sample synthesised at 100 °C. Rietveld analysis of the diffraction data from the sample at room temperature suggested the sample contained 2.4(1) wt% MnF₂, and revealed an additional small (1.3(1) wt%) impurity of 6H-CsMnF₃ which was not detected by laboratory XRD. The remainder (96.3(1) wt%) was cubic CsMnF₃ and these three phases account for all observed diffraction peaks (Figure 1a). Upon cooling to 100 K, the main phase remains cubic with a contraction of the lattice parameter *a* (Figure 1c inset). A quartz capillary filled with a specimen from the same sample had slightly higher refined weight fractions of MnF₂ and 6H-CsMnF₃ at room temperature (6.63(7) wt% and 2.93(3) wt%, respectively). Upon heating, no significant changes are observed up to 300 °C.

Above 300 °C, a phase transition from cubic CsMnF₃ to 6H-CsMnF₃ occurs, which is complete by 500 °C (773 K, Figure 1b,c). This shows that the cubic polymorph is metastable and it is unlikely that it can be synthesised by a conventional solid-state reaction at ambient

^aDepartment of Chemistry, University of Warwick, Gibbet Hill Road, Coventry, CV4 7AL, U.K. Email: r.i.walton@warwick.ac.uk or m.senn@warwick.ac.uk

^bInstitut Laue-Langevin, 71 Avenue des Martyrs, CS20156, 38042 Grenoble Cédex 9, France.



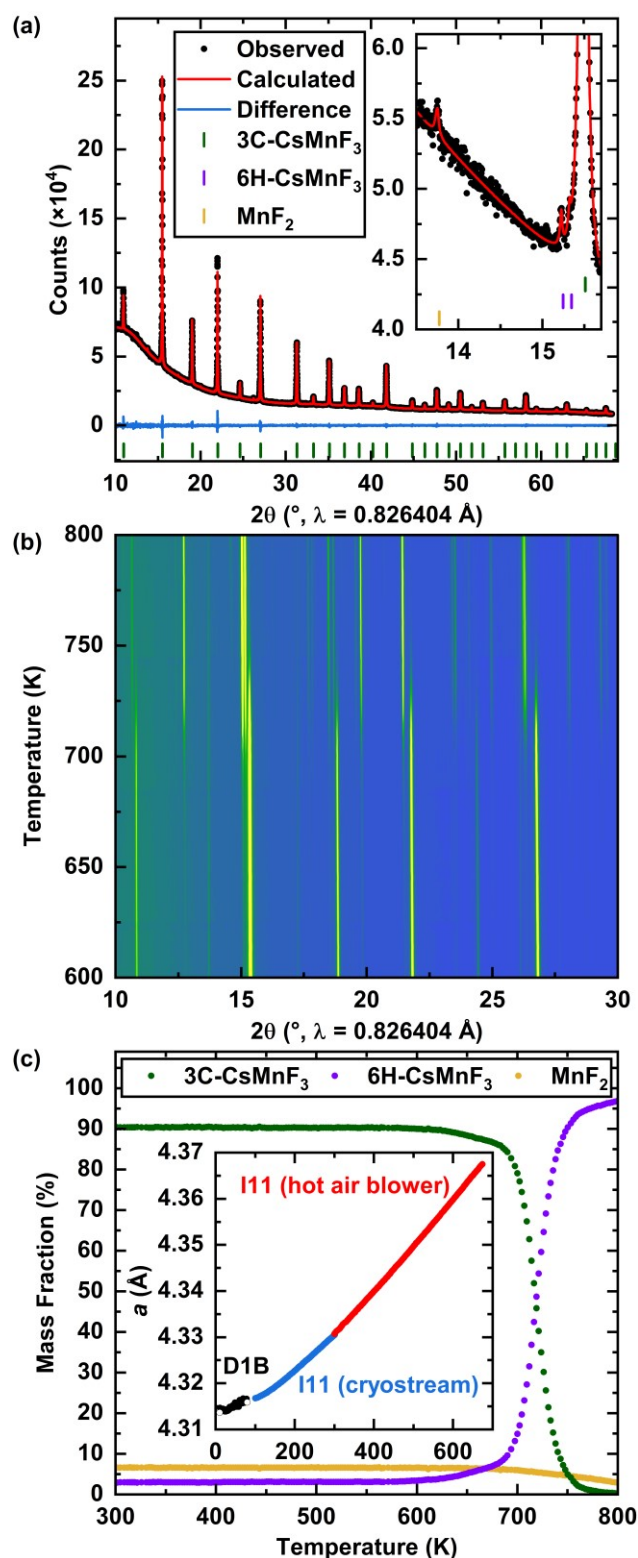


Figure 1. (a) Three-phase Rietveld fit to synchrotron XRD collected from a sample of cubic (3C) CsMnF₃ at 300 K (in borosilicate capillary). Tick marks for 6H-CsMnF₃ and MnF₂ impurities omitted for clarity. Inset shows weak peaks from impurity phases (with tick marks shown). (b) Synchrotron X-ray diffraction contour plot measured as a function of temperature, shown over phase transition temperature region. (c) Refined mass fractions of crystalline phases from sample (in quartz capillary) using synchrotron XRD upon heating. Inset shows refined lattice parameter, a , as a function of temperature measured using three diffraction experiments. For D1B, open and closed symbols were measured using a short (1.28 Å) and long (2.52 Å) neutron wavelengths, respectively.

pressure. Additionally, the amount of MnF₂ gradually decreases from ~400 °C, with additional, unidentified peaks appearing from 450 °C, which is likely to be caused by reaction with air in the capillary or with the quartz capillary (Figure S2).

The Goldschmidt tolerance factor, t , of CsMnF₃ is 1.06 is close to a cubic – hexagonal threshold, so it is not obvious from t alone which polymorph is likely to form. Previous high temperature syntheses of the hexagonal polymorph, and the phase transition observed here from cubic to 6H-CsMnF₃ upon heating, suggest that latter is the most thermodynamically stable polymorph. However, the isolation of the cubic polymorph from low temperature solution syntheses may suggest that the formation of face-sharing MnF₆ octahedral environments has a significantly higher activation energy, likely due to the shorter cation-cation distances and hence repulsion.¹⁴

The magnetic susceptibility of cubic CsMnF₃ shows variation as a function of temperature that is indicative of antiferromagnetic order, with a Néel temperature (T_N) of approximately 70 K (Figure 2a). This is in contrast to 6H-CsMnF₃, which has a complex magnetic structure with antiferromagnetic and ferrimagnetic exchange pathways that has not been fully resolved.^{15–17} A linear fit to the high temperature, paramagnetic region ($350 \text{ K} \leq T \leq 400 \text{ K}$) of the inverse molar susceptibility gives a good agreement and can be interpreted by the Curie-Weiss law (Figure 2a). This gives a Curie-Weiss temperature, ϑ_{CW} , of -94.5(8) K, which indicates net antiferromagnetic interactions and an effective moment per Mn²⁺ ion, μ_{eff} , of 6.29(2) μ_B . High spin Mn²⁺ has no orbital angular momentum ($L = 0$) and its spin-only moment is 5.92 μ_B . A 6.3 wt% MnF₂ impurity is sufficient to account for the discrepancy between μ_{eff} and the spin-only value, which is concordant with the mass fraction obtained by Rietveld refinement against powder synchrotron XRD from the sample in a quartz capillary (refined to 6.63(7) wt%). The literature shows that the μ_{eff} of octahedral high spin Mn²⁺ (and Fe³⁺, another ^{6S} ion) has been reported to be between 6.1 μ_B and 6.4 μ_B in several other fluorides, oxides and phosphates.^{15, 18–26} This divergence has sometimes been attributed to short range correlation persisting above T_N , or slight deviation from an ideal octahedral environment. These effects are unlikely to be the cause of a larger-than-expected μ_{eff} in cubic CsMnF₃; it has a regular octahedral environment for Mn (on average) and the Curie-Weiss fit was carried out across a temperature range of 350 – 400 K, much greater than T_N (~70 K).

Variable temperature neutron powder diffraction data²⁷ were collected using the D1B²⁸ powder diffractometer (Institut Laue-Langevin, France). To prepare the large powder sample (~5 g) for neutron diffraction, a synthesis scaled up by a factor of 10 was employed (see Experimental). This sample was found to contain an increased amount of MnF₂ (18.2 wt%, by Rietveld analysis of neutron powder diffraction) compared to the original sample. When cooled below T_N , CsMnF₃ remains apparently cubic, though several magnetic superstructure peaks develop in the neutron diffraction pattern at $d = 4.98 \text{ \AA}$, 2.06 \AA , 1.98 \AA and 1.67 \AA , as well as the main antiferromagnetic superstructure²⁹ peak (100) from MnF₂ at $d = 4.87 \text{ \AA}$ (partly overlapping from the cubic CsMnF₃ peak, Figure 2b), which has a similar T_N . A fit to the neutron diffraction pattern at 10 K (Figure 2c) shows cubic CsMnF₃ has G-type antiferromagnetic ordering at 10



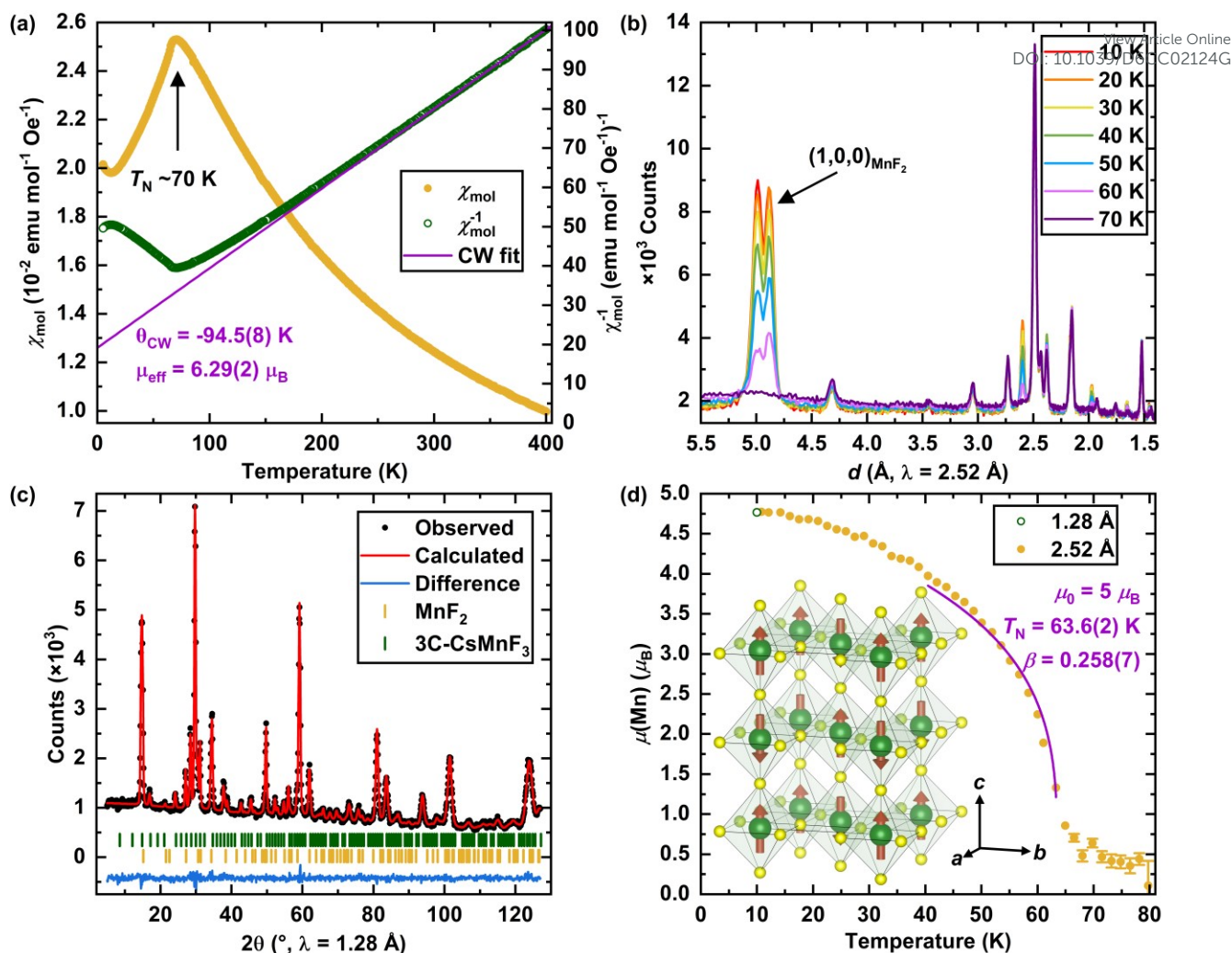


Figure 2. (a) Molar magnetic susceptibility of cubic CsMnF_3 as a function of temperature in an applied field of 1000 Oe, with a Curie-Weiss (CW) fit to the inverse molar magnetic susceptibility. (b) Variable temperature neutron diffraction in 10 K increments, plotted in d -space. (c) Two-phase (cubic CsMnF_3 and MnF_2) magnetic Rietveld fit to neutron powder diffraction data at 10 K. Tick marks for both phases include magnetic superstructure peaks (d) Refined Mn^{2+} moment in cubic CsMnF_3 as a function of temperature with a fit using a critical power law (see text). Inset shows the G-type antiferromagnetic ordering in cubic CsMnF_3 structure, with Cs ions omitted for clarity. *n.b.* All neutron powder diffraction data presented in (b-d) were measured from a different sample containing ~ 18 wt% MnF_2 .

K, with a moment of $4.77(2) \mu_B$ (Figure 2d, inset). The moment direction could not be uniquely determined from the powder data. This model was used to fit to the variable temperature data upon heating to 80 K, with lattice parameter a slightly increasing (Figure 1b) and the Mn magnetic moment, $\mu(\text{Mn})$, undergoing an exponential decay (Figure 2d). Close to the T_N ($40 \text{ K} < T < 65 \text{ K}$), $\mu(\text{Mn})$ can be fitted using a critical power law, with the saturated moment, μ_0 , fixed at the 2S value of $5 \mu_B$. The fit yields a T_N of $63.6(2)$ K and a critical exponent, β , of $0.258(7)$, suggesting a significant deviation from a mean field system ($\beta = 0.5$) or simple 3D Heisenberg or Ising antiferromagnetic systems ($\beta = 0.365$ and 0.325 , respectively).³⁰ A β close to 0.25 may suggest a tricritical point.³¹

Goldschmidt's tolerance factor³² (t) is a geometric relationship used for predicting the structure of ABX_3 compositions based on the radii of constituent ions. The threshold values of t have been largely determined from the rich family of oxide perovskites, though fluoride perovskites, ABF_3 , largely obey the same trend; because of the similar size and hardness of the fluoride and oxide anions (whilst other, softer halide ions display significant deviation from these values).³³ The NaBF_3 perovskites ($B = \text{Mn-Ni}$) have values of t

between 0.89 and 0.96 and all adopt an orthorhombically distorted, GdFeO_3 -type perovskite structure,⁹ whilst the analogous KBF_3 perovskites are all cubic³⁴ (at room temperature³⁵⁻³⁷) and range in t between 0.97 and 1.05, and the CsBF_3 perovskites have $t \geq 1.06$ and all are reported to adopt a hexagonal polytype when prepared by solid state, high-temperature synthesis.³⁸

Figure 3 compares the crystal structures of the two polymorphs studied here, showing the different connectivity of the Mn-centred octahedra. The application of pressure to hexagonal perovskites has been found to destabilise the B cations in face-sharing octahedra due to B-B repulsion.^{39, 40} In particular, Kafalas and Longo¹² found the CsBF_3 ($B = \text{Mg, Mn-Ni, Zn}$) hexagonal perovskites convert to hexagonal polytypes with an increasing proportion of ccp layers with application of pressure, with a transition from the 6H to the cubic ("3C") polymorph seen in CsMnF_3 and CsFeF_3 when quenched from 700°C at 30 and 80 kbar, respectively, whose tolerance factors (1.06 and 1.07 respectively) are closest to the cubic – hexagonal threshold. A synthesis of an impure sample cubic nanocrystalline CsMnF_3 was recently reported by Fellner and Lauria⁴¹ from Mn(II) acetate and CsF (1 : 3 ratio, respectively) in a mixture of oleic acid and octadecene at



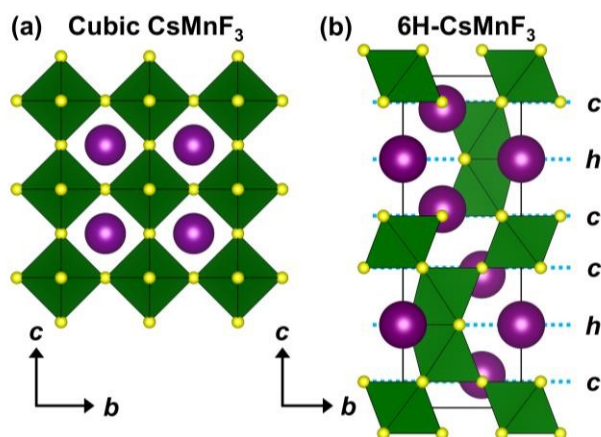


Figure 3. (a) Cubic and (b) 6H- CsMnF_3 with purple Cs cations, green MnF_6 octahedra and yellow F anions. In (b), the packing of the CsF_3 layers are denoted either c or h to denote cubic or hexagonal close packing, respectively.

160 °C. This sample was contaminated with a significant amount of an acid fluoride phase $\text{Cs}_2\text{H}_3\text{F}_5$ (though the diffraction pattern of $\text{Cs}_2\text{H}_3\text{F}_5$ has been indexed to a face-centred cubic cell, its crystal structure has not previously been determined, making quantitative analysis impossible). The AC magnetic susceptibility as a function of temperature of the mixed CsMnF_3 - $\text{Cs}_2\text{H}_3\text{F}_5$ sample suggested antiferromagnetic ordering occurred at a low temperature (<60 K, though this can be affected by the oscillating field frequency in AC susceptibility measurements⁴²). Scanning electron microscopy (SEM) from the sample prepared by our synthesis route shows crystallites with a predominant rod-like morphology (Figure 4a) with widths of $\sim 0.1 \mu\text{m}$ and lengths of $\sim 0.4 \mu\text{m}$, contrasting with the 5 nm crystallites observed in the sample reported by Fellner and Lauria.⁴¹ When the sample was heated to 748 K (475 °C) under N_2 for 1 hr, 6H- CsMnF_3 is produced with crystallites that retain the approximate rod-like morphology though with a more-rounded shape and an increase in crystallite size (Figure 4b).

In summary, we have prepared high purity cubic CsMnF_3 by a solvothermal reaction in ethylene glycol that allows its phase transitions and magnetic behaviour to be studied in detail. We have shown that it converts to the thermodynamic 6H polymorph upon heating to ~ 450 °C, demonstrating its metastability. Magnetic susceptibility and powder neutron diffraction show that the sample is a G-type antiferromagnet with $T_N \sim 70$ K. The preparative chemistry developed could be applicable to other transition-metal fluorides with the prospect of discovery of novel compositions and crystal structures, with control of crystal morphology.

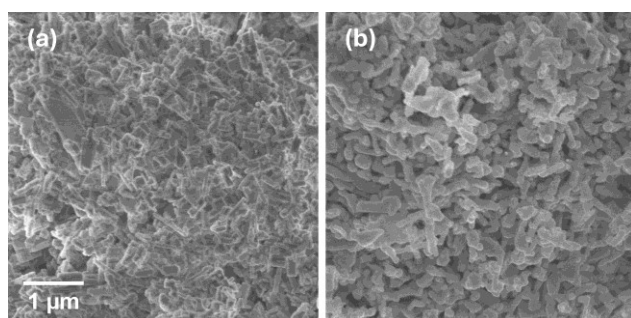


Figure 4. SEM images of (a) as-made cubic CsMnF_3 and (b) 6H- CsMnF_3 made by heating of the cubic polymorph. Scale bar the same for both.

Data availability

View Article Online

DOI: 10.1039/D6CC02124G

All data generated or analysed during this study are included in this article and the supplementary information (SI). Data from ILL available at <http://dx.doi.org/10.5291/ILL-DATA.5-24-770>. Electronic supporting information is available.

Conflicts of interest

The authors declare that they have no known competing financial interests or personal relationships that could have appeared to influence the work reported in this paper.

Acknowledgements

R.I.W. and M.S.S. acknowledge the Leverhulme Trust for a research project grant (Grant No. RPG-2022-22). M.S.S. acknowledges the Royal Society for a fellowship (UF160265 and URF\R\231012). Initial sample characterisation was performed via the Warwick X-ray and Microscopy Research Technology Platforms. We thank Professor Martin R. Lees for access to SQUID magnetometer. Synchrotron powder XRD was supported by the Diamond Light Source Oxford-Warwick BAG CY39378-4, and the Institut Laue-Langevin provided neutron diffraction under experiment 5-24-770 (doi:10.5291/ILL-DATA.5-24-770). We thank Putthachat Sinted for assistance with neutron diffraction measurement and Andrew Unsworth for electron microscopy support.

References

- Walton, R. I. *Chem. Eur. J.* 2020, **26**, 9041-9069.
- Zhu, J.; Li, H.; Zhong, L.; Xiao, P.; Xu, X.; Yang, X.; Zhao, Z.; Li, J. *ACS Catalysis* 2014, **4**, 2917-2940.
- Si, C.; Zhang, W.; Lu, Q.; Guo, E.; Yang, Z.; Chen, J.; He, X.; Luo, J. *Catalysts* 2022, **12**, 601.
- Xue, X.; Li, B. *Nanomaterials (Basel)* 2025, **15**, 472.
- Modeshia, D. R.; Darton, R. J.; Ashbrook, S. E.; Walton, R. I. *Chem. Commun.* 2009, 68-70.
- Clark, I.; Takeuchi, T.; Ohtori, N.; C. Sinclair, D. *J. Mater. Chem.* 1999, **9**, 83-91.
- Tressaud, A. *J. Fluorine Chem.* 2025, **281**, 110374.
- Yan, Q.; Xu, H.; Hoang, K.; Zhou, X.; Kidkhunthod, P.; Lightfoot, P.; Yao, W.; Tang, Y. *Appl. Phys. Lett.* 2022, **121**.
- Crawford, C. A.; Hiley, C. I.; Gainza, J.; Ritter, C.; Walton, R. I.; Senn, M. S. *Phys. Rev. B* 2025, **112**, 035150.
- Crawford, C. A.; Hiley, C. I.; Scott, C. A. M.; Ritter, C.; Lees, M. R.; Bristowe, N. C.; Walton, R. I.; Senn, M. S. *Inorg. Chem.* 2024, **63**, 9184-9194.
- Ben Yahia, H.; Shikano, M.; Tabuchi, M.; Kobayashi, H.; Avdeev, M.; Tan, T. T.; Liu, S.; Ling, C. D. *Inorg. Chem.* 2014, **53**, 365-374.
- Longo, J. M.; Kafalas, J. A. *J. Solid State Chem.* 1969, **1**, 103-108.
- Thompson, S. P.; Parker, J. E.; Potter, J.; Hill, T. P.; Birt, A.; Cobb, T. M.; Yuan, F.; Tang, C. C. *Rev. Sci. Instrum.* 2009, **80**.
- Mitchell, R. H. *Perovskites: Modern and Ancient*; Almaz Press, 2002.
- Zhu, X.; Zhao, Y.; Zhang, S.; Wu, J.; Shao, D.; Song, E.; Zhang, Q.; Yin, C.; Ye, S. *The Journal of Physical Chemistry C* 2021, **125**, 27800-27809.
- Yamaguchi, Y.; Sakuraba, T. *J. Phys. Soc. Jpn.* 1975, **38**, 1011-1019.
- Oleaga, A.; Salazar, A.; Bunkov, Y. M. *Journal of Physics : Condensed Matter* 2014, **26**, 096001.



¹⁸Li, T.; Clulow, R.; Bradford, A. J.; Lee, S. L.; Slawin, A. M. Z.; Lightfoot, P. *Dalton Trans.* 2019, **48**, 4784-4787.

¹⁹Li, T.; Bradford, A. J.; Lee, S. L.; Lightfoot, P. *Chem. Mater.* 2024, **36**, 5228-5237.

²⁰Winterstein, A.; Akamatsu, H.; Möncke, D.; Tanaka, K.; Schmidt, M. A.; Wondraczek, L. *Opt. Mater. Express* 2013, **3**, 184-193.

²¹Sanders, M. B.; Krizan, J. W.; Plumb, K. W.; McQueen, T. M.; Cava, R. J. *J. Phys.: Condens. Matter* 2017, **29**, 045801.

²²Zatsiupa, A. A.; Bashkurov, L. A.; Troyanchuk, I. O.; Petrov, G. S.; Galyas, A. I.; Lobanovskii, L. S.; Trukhanov, S. V.; Sirota, I. M. *Inorg. Mater.* 2013, **49**, 616-620.

²³Matan, K.; Bartlett, B. M.; Helton, J. S.; Sikolenko, V.; Mat'áš, S.; Prokeš, K.; Chen, Y.; Lynn, J. W.; Grohol, D.; Sato, T. J.; et al. *Phys. Rev. B* 2011, **83**, 214406.

²⁴Solana-Madruga, E.; Dos santos-García, A. J.; Arévalo-López, A. M.; Ávila-Brandé, D.; Ritter, C.; Attfield, J. P.; Sáez-Puche, R. *Dalton Trans.* 2015, **44**, 20441-20448.

²⁵Zhu, X.; Meng, S.; Zhao, Y.; Zhang, S.; Zhang, J.; Yin, C.; Ye, S. *J. Phys. Chem. Lett.* 2020, **11**, 9587-9595.

²⁶Ueda, H.; Inamori, T.; Taguchi, A.; Michioka, C.; Yoshimura, K. *J. Phys. Soc. Jpn.* 2021, **91**, 014704.

²⁷Sinted, P.; Crawford, C. A.; Hiley, C. I.; Nassif, V.; Ritter, C.; Senn, M. S.; Walton, R. I. *Investigation of Phase Transitions of Mixed A-site Perovskites $K_{1-x}Rb_xMnF_3$ ($x \leq 1$)*. Institut Laue-Langevin, 2025, doi:10.5291/ILL-DATA.5-24-770.

²⁸Orench, I. P.; Clergeau, J. F.; Martínez, S.; Olmos, M.; Fabelo, O.; Campo, J. J. *J. Phys. Conf. Ser.* 2014, **549**, 012003.

²⁹Yamani, Z.; Tun, Z.; Ryan, D. H. *Can. J. Phys.* 2010, **88**, 771-797.

³⁰Stanley, H. E. *Introduction to phase transitions and critical phenomena*; Oxford University Press, 1987.

³¹Massa, N. E.; del Campo, L.; de Souza Meneses, D.; Echegut, P.; Fabbris, G. F. L.; Azevedo, G. d. M.; Martínez-Lope, M. J.; Alonso, J. A. *J. Appl. Phys.* 2010, **108**.

³²Goldschmidt, V. M. *Naturwissenschaften* 1926, **14**, 477-485.

³³Travis, W.; Glover, E. N. K.; Bronstein, H.; Scanlon, D. O.; Palgrave, R. G. *Chem. Sci.* 2016, **7**, 4548-4556.

³⁴Clark, L.; Lightfoot, P. 13 - Magnetic Properties of Transition Metal Fluoride Perovskites. In *Photonic and Electronic Properties of Fluoride Materials*, Tressaud, A., Poeppelmeier, K. Eds.; Elsevier, 2016; pp 261-284.

³⁵Knight, K. S.; Khalyavin, D. D.; Manuel, P.; Bull, C. L.; McIntyre, P. J. *Alloys Compd.* 2020, **842**, 155935.

³⁶Knox, K. *Acta Crystallogr.* 1961, **14**, 583-585.

³⁷Hirakawa, K.; Hirakawa, K.; Hashimoto, T. *J. Phys. Soc. Jpn.* 1960, **15**, 2063-2068.

³⁸Schmidt, R. E.; Welsch, M.; Kummer-Dörner, S.; Babel, D. Z. *Anorg. Allg. Chem.* 1999, **625**, 637-642.

³⁹Oka, K.; Azuma, M.; Hirai, S.; Belik, A. A.; Kojitani, H.; Akaogi, M.; Takano, M.; Shimakawa, Y. *Inorg. Chem.* 2009, **48**, 2285-2288.

⁴⁰Li, Y.; Cheng, J.; Alonso, J. A.; Goodenough, J. B.; Zhou, J. *Inorg. Chem.* 2017, **56**, 8187-8194.

⁴¹Fellner, M.; Lauria, A. J. *Sol-Gel Sci. Technol.* 2023, **107**, 259-268.

⁴²Topping, C. V.; Blundell, S. J. *J. Phys.: Condens. Matter* 2019, **31**, 013001.

View Article Online
DOI: 10.1039/D6CC02124G



View Article Online
DOI: 10.1039/D6CC02124G

Data availability statement

All data generated or analysed during this study are included in this article and the supplementary information (SI). Data from ILL available at <http://dx.doi.org/10.5291/ILL-DATA.5-24-770>. Electronic supporting information is available.

